Role of Flavin Mononucleotide in the Thermostability and Oligomerization of Escherichia coli Stress-Defense Protein WrbA†

Antonino Natalello,‡ Silvia Maria Doglia,‡ Jannette Carey,§ and Rita Grandori*,‡,||

Department of Biotechnology and Biosciences, University of Milano-Bicocca, Milan, Italy, Department of Chemistry, Princeton University, Washington Road, Princeton, New Jersey, and Institute of Organic Chemistry, Johannes Kepler University, Linz, Austria

Received August 28, 2006; Revised Manuscript Received November 14, 2006

ABSTRACT: WrbA is an oligomeric flavodoxin-like protein that binds one molecule of flavin mononucleotide (FMN) per monomer and whose redox activity is implicated in oxidative stress defense. WrbA thermostability and oligomerization in the presence and absence of bound FMN were investigated using complementary biophysical methods. Infrared spectroscopy indicates similar structures for apo and holoWrbA. FMN binding has a dramatic effect on WrbA thermal stability, shifting the T_m by ∼40 °C. Upon denaturation, the protein forms insoluble aggregates that lack native secondary structure and have no bound FMN. Circular dichroism (CD) reveals that the thermal unfolding of apo and holoWrbA proceeds via the formation of an aggregation-prone intermediate that retains substantial secondary structure but has lost the native configuration of the active site. This intermediate persists in solution up to 100 °C at micromolar concentrations. A similar partially folded state is populated during chemical denaturation with guanidinium chloride, but accumulation of the intermediate is evident only in the absence of FMN. The results also suggest that WrbA maintains some interaction with FMN in its partially folded state, despite the loss of the induced CD signal of FMN. On the basis of these data, the unfolding process can be depicted as follows: native holoprotein → holointermediate → apointermediate → insoluble aggregate. Mass spectrometry shows that FMN promotes WrbA association into tetramers, which are more thermoresistant than dimers or monomers, suggesting that multimerization underlies the FMN effect on WrbA thermostability. This study illustrates the utility of analyzing conformational transitions and intermolecular interactions using methods that probe the liquid, solid, and gas phases.

The 21 kDa protein WrbA from *E. coli* is the founding member of a highly conserved family of proteins implicated in cellular responses to altered redox conditions and to different kinds of stress (*1*). Its expression is enhanced in the stationary phase under transcriptional control by *RpoS* (*2*), the central regulator of the general stress response (*3*). WrbA appears to be coregulated with Dps (*PexB*), a nonspecific DNA binding protein that protects DNA against chemical damage during oxidative stress (*4*). Consistent with a role in oxidative stress defense, WrbA is a redox-active protein (*5*) that binds flavin mononucloetide (FMN[1]) as its physiological cofactor (*6*). A recent report identifies the WrbA proteins from *E. coli* and *Archeoglobus fulgidus* as NAD(P)H/quinone oxidoreductases (*7*), as previously documented also for the secreted homologue from *Gloeophyllum trabeum* (*8*). Although the latter has a role in extracellular Fenton chemistry to support wood degradation, the intracellular homologues in *E. coli* and other organisms could be involved in quinone detoxification (*7*).

E. coli WrbA was reported to co-purify and co-immunoprecipitate with the tryptophan repressor (TrpR), hence the name tryptophan(*W*)-*r*epressor-*b*inding protein *A* (*2*). However, the protein has no specific effect on TrpR−DNA binding (*6*). Although a direct connection to tryptophan repressor, therefore, appears unlikely, a link to tryptophan metabolism remains possible, perhaps involving indole, a well-known signalling molecule in stationary phase (*9*). Indole-3-acetic acid was recently reported to improved *E. coli*'s defense to stress (*10*). Further testifying to a role in stress response for this protein family, the WrbA protein from *S. pombe*, called p25, accumulates upon the exposure of cells to hydrogen peroxide (*11*). Overexpression of p25 correlates with a pleiotropic phenotype that includes resistance to staurosporine, brefeldin A, caffeine, cycloheximide, heavy metals, and oxidative stress (*11*−*13*). WrbA transcription in yeast is positively regulated by the redox-sensitive AP-1-like transcription factors (*14*), whose subunits are homologous to the oncogene products *jun* and *fos* (*15*). The WrbA sequence from *S. cerevisiae* contains signals for palmitoylation and carboxymethylation (*16*), and the protein has been localized at the plasma membrane by immunofluorescence (Petsko, G., personal communication).

† This work was supported by Grant T135 from the Austrian Science Foundation (FWF) to R.G, Grant NSF-INT03-09049 to J.C., and F.A.R. (Fondo d'Ateneo per la Ricerca) to S.M.D.

* To whom correspondence should be addressed. Tel. +39 02 64483363. Fax: +39 02 64483565. E-mail: rita.grandori@unimib.it.

‡ University of Milano-Bicocca.

§ Princeton University.

|| Johannes Kepler University.

[1] Abbreviations: FMN, flavin mononucleotide; CD, circular dichroism; FT-IR, Fourier-transform infrared spectroscopy; UV, ultraviolet; GuHCl, guanidinium chloride; CSD, charge-state distribution; ESI-MS, electrospray-ionization mass spectrometry; SD, standard deviation.

10.1021/bi061769c CCC: $37.00 © 2007 American Chemical Society
Published on Web 12/19/2006

WrbA proteins are related by remote homology to flavodoxins (*1*), but *E. coli* WrbA displays a much lower affinity for FMN than many flavodoxins (K_d in the range of 10^{-6} M vs $10^{-7}-10^{-10}$ M for flavodoxins) (*6*, *17*, *18*). This difference may reflect altered interactions with the flavin cofactor at the protein active site (*19*). Unlike flavodoxin (*20*), WrbA is oligomeric, with a monomer−dimer−tetramer equilibrium (*6*), and it transfers pairs of electrons rather than single electrons (*5*). The recently reported crystal structures of *Deinococcus radiodurans* and *Pseudomonas aeruginosa* apo and holoWrbA proteins (*21*) reveal an α/β twisted open-sheet fold in a tetrameric assembly and one FMN bound per protein subunit. Tetramerization is promoted by a helix that displays high sequence conservation within the WrbA family but is poorly conserved between the WrbA and flavodoxin families (*1*). Like the long-chain flavodoxins, β5 of WrbA is interrupted by a loop insertion. Both crystallographic (*21*) and CD (*6*) data indicate that no major conformational changes are associated with FMN binding to WrbA. The crystal structure reveals two distinct subunit interfaces that bury 2423 and 1601 Å^2 of total surface area. Intersubunit contacts at the smaller interface are mediated by FMN. On the basis of this feature, it has been suggested (*21*) that tetramerization might be modulated by the cofactor. In the present study, the role of FMN in WrbA stability and oligomerization is investigated by means of complementary biophysical methods.

MATERIALS AND METHODS

Protein Purification. WrbA was expressed in *E. coli* strain CY15071 as previously described (*6*). Cells overexpressing WrbA were collected from 1 L of culture and resuspended in buffer T (20 mM Tris-HCl at pH 8), containing 10 mM EDTA and 1 mM phenylmethylsulfonyl fluoride. Lysozyme was added to 0.2 mg/mL, and after incubation for 20 min at room temperature, cells were sonicated and centrifuged at 30 000*g* for 30 min. The soluble fraction was loaded onto a 20 mL DEAE-cellulose column (Amersham Biosciences, Uppsala, Sweden) equilibrated with buffer T. Proteins were eluted by a linear gradient of NaCl from 0 to 1 M in buffer T at a flux of 1 mL/min. The pool of yellow fractions containing WrbA was dialyzed against buffer T and loaded on a 5 mL Affi-gel Blue column (Bio-Rad, CA) equilibrated in the same buffer. After washing, the column was developed by a linear gradient of NaCl from 0 to 1 M in buffer T at 0.5 mL/min. The pool of fractions containing pure WrbA was dialyzed against buffer P (20 mM sodium phosphate at pH 7.2) or against deionized water, concentrated in a centrifugal filter device (Amicon, Millipore, Bedford, MA) and stored in aliquots at −20 °C. The purity and identity of WrbA were established by SDS−PAGE and ESI-MS. To minimize differences in the history of apo and holoprotein samples, the latter were always prepared by the addition of a molar excess of FMN, as specified, to freshly thawed aliquots of the apoprotein stock solution.

Fourier-Transform Infrared Spectroscopy (FT-IR). FT-IR absorption spectra of 1.3 mM WrbA in buffer P, with or without 2 mM FMN, were recorded on a FTS-40A spectrometer (Bio-Rad, Digilab Division, Cambridge, MA) equipped with a deuterated triglycine sulfate detector and an air dryer purging system. For FT-IR transmission measurements, 20 μL of sample solution were deposed between two BaF_2 windows separated by a 15 μm Teflon spacer in a temperature-controlled cell (Wilmad, Buena, NJ). Spectra were recorded at 2 cm^{-1} resolution, 5 kHz scan speed, with 256 interferograms co-added, and with triangular apodization. For thermal denaturation experiments, the temperature was varied at a linear rate of 0.2 °C/min from 27 to 100 °C. The FT-IR spectra of the protein were obtained after subtraction of the buffer and vapor spectra obtained under identical conditions (*22*). Second-derivative analysis was performed because minima in the derivative spectrum allow the identification of the different components in the Amide I and Amide II regions (*23*). Derivative spectra were obtained by the Savitsky−Golay method (third grade polynomial, 5-point smoothing), after binomial 11-point smoothing of the spectrum using the GRAMS/32 software (Galactic Industries Corporation, Salem, NH).

Circular Dichroism (CD). CD spectra were recorded on a Jasco (Easton, MD) J-810 spectropolarimeter. The samples contained 30 μM pure WrbA in buffer P. Holoprotein samples also contained 180 μM FMN. Spectra in the far-UV region (180−250 nm) were collected at 20 °C in a 0.1 cm path length quartz cell at a scanning speed of 20 nm/min with 3-scan averaging. In the near-UV/visible region (340−500 nm), spectra were acquired using a 1 cm path length quartz cell at 20 °C, a scanning speed of 50 nm/min, and at 3-scan averaging. For thermal unfolding experiments, the sample temperature was varied from 20 to 100 °C at three heating rates: 0.2, 0.45, or 1 °C/min. CD protein spectra are presented without smoothing.

Electrospray-Ionization Mass Spectrometry (ESI-MS). Mass spectra were recorded in positive-ion mode on a Mariner time-of-flight mass spectrometer from Applied Biosystems (Darmstadt, Germany) using a nanospray ion source. Au/Cd coated borosilicate capillaries (inner diameter of the emitter tip is ∼1 μm) were purchased from Proxeon (Odense, Denmark). The instrumental settings were as follows: spray-tip potential, 1700 V; nozzle-to-skimmer potential, 140 V; curtain-gas (N_2) flow rate, 0.6 L/min; and nozzle temperature, 85 °C unless otherwise stated. The integration time was 6 s per spectrum. The electrospray capillary was kept at room temperature. The reported traces are averaged over at least 20 spectra. Samples were prepared in 1 mM ammonium acetate at pH 4 (pH adjusted by the addition of formic acid) no longer than 2 h before analysis.

RESULTS

Secondary Structure Analysis by FT-IR. Protein FT-IR spectra display two main absorption regions, called Amide I and Amide II, which are due to vibrational modes of the peptide group. Absorption in the Amide I region (1600 to 1700 cm^{-1}) arises from CO stretching vibrations, whose frequency is sensitive to protein secondary structure (*23*−*26*). Absorption in the Amide II region (1520 to 1600 cm^{-1}) is mainly ascribable to NH bending modes, with contributions from CN, CO, and CC vibrations. Different components of protein secondary structure have been assigned in the Amide I region on the basis of the reference spectra of model compounds and proteins of known structure (*26*−*28*). Due to its complexity, the Amide II region is less informative about protein conformation (*25*).

FT-IR absorption spectra were measured at room temperature for 1.3 mM apo or holoWrbA in buffer P. Holoprotein

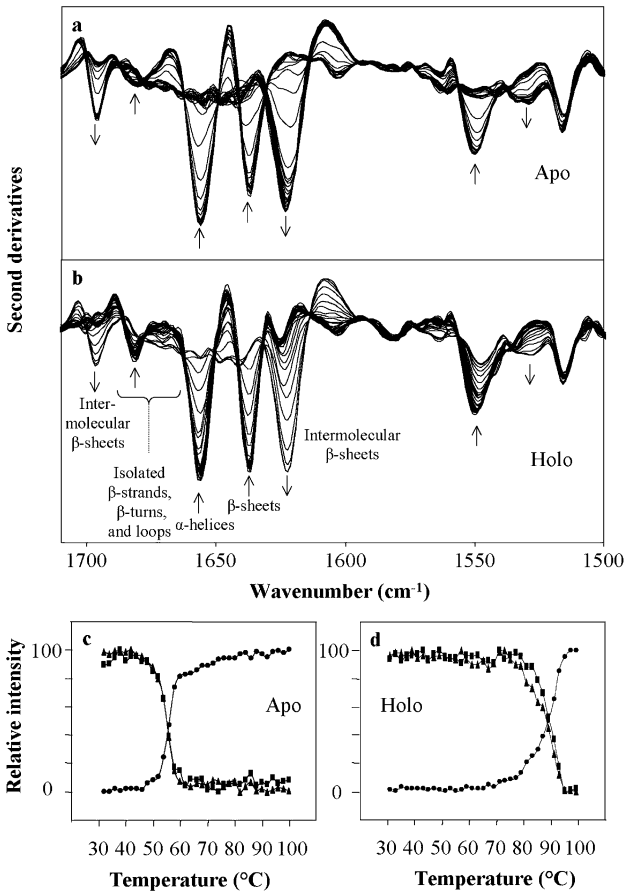

FIGURE 1: Thermal unfolding monitored by FT-IR. (a, b) Second-derivative FT-IR spectra of 1.3 mM apo and holoWrbA at selected temperatures between 27 and 100 °C. The arrows indicate the direction of changes with increasing temperature. (c, d) Thermal profiles at selected wavenumbers. (▲), 1655.5 cm^{-1} (α-helices); (■), 1636.9 cm^{-1} (intramolecular β-sheets); (●), 1622.6 cm^{-1} (intermolecular β-sheets). Intensity is normalized relative to the magnitude of total signal change at each wavelength. The reported values are from one representative experiment. Variability, measured as the distance from the mean of three experiments, is within 4% of the values shown.

samples contained 2 mM FMN, affording >98% occupancy of the bound state according to the equilibrium constant of 2 μM determined previously (*6*). The second derivatives of the FT-IR absorption, corrected for buffer absorption and vapor contributions, are shown in Figure 1. Band assignment is summarized in Table 1. Major contributions of the α-helix and β-sheet structures are observed in the Amide I region (1700−1600 cm^{-1}), as expected for a protein of this fold class. The α-helix and β-sheet bands (around 1655.5 and 1636.9 cm^{-1}, respectively) map at approximately the same wavenumbers in the apo (Figure 1a) and holo (Figure 1b) proteins, and their intensities are not affected by the presence of FMN. Thus, WrbA, like flavodoxin, can adopt a native fold in the absence of the cofactor, consistent with CD (*6*) and crystallographic (*21*) results.

Nevertheless, minor spectral changes accompany the addition of FMN. In holoWrbA, all of the Amide I and Amide II components are sharper than those in apoWrbA, suggesting a global response of the protein to the binding of the cofactor. Sharpening of the spectrum indicates that the dynamics and/or conformational heterogeneity are reduced (*25*, *29*). In particular, the bands at ∼1695, ∼1682, and ∼1625 cm^{-1} are more pronounced in the holoprotein spectrum. The band at ∼1682 cm^{-1} can be assigned to β-turns or isolated β-strands (*26*, *29*) and, therefore, could reflect the interaction of FMN with β-turns and loops at the active site (*21*). The bands at ∼1695 and ∼1625 cm^{-1} reflect intermolecular hydrogen bonding (*26*, *30*), consistent with the presence of protein assemblies, which appear to be present at higher relative amounts in the holoprotein. These changes in the IR spectrum thus provide a first suggestion that FMN binding might affect protein subunit interactions, an effect that is further investigated in this work by other techniques.

Table 1: FT-IR Secondary Structure Assignment for the Native WrbA

apo band position (cm^{-1})[a]		holo band position (cm^{-1})[a]		
mean	SD	mean	SD	assignment (*23*, *26*, *29*)
1695.4	0.8	1695.2	0.7	intermolecular β-sheets
1682.5	1.5	1681.5	0.1	isolated β-strands, β-turns, and loops
1675.0	1.7	1672.8	0.6	isolated β-strands, β-turns, and loops
1655.2	0.7	1655.8	0.1	α-helices
1636.6	0.3	1637.2	0.1	intramolecular β-sheets
∼1625		1625.3	0.4	intermolecular β-sheets

[a] Mean and standard deviation (SD) refer to the values observed in three independent measurements.

Thermal Unfolding of WrbA Apo and Holoprotein Monitored by FT-IR. Figure 1a also shows second-derivative FT-IR spectra of apoWrbA as a function of temperature. Samples were heated at a linear rate of 0.2 °C/min, each spectrum being collected within a temperature interval of 2°. No changes in the spectrum are observed up to 45 °C. Above this temperature, a progressive decrease in band intensity is observed for both the α-helix at 1655.5 cm^{-1} and the intramolecular β-sheet at 1636.9 cm^{-1}. At the same temperature, a new band develops at 1622.6 cm^{-1}, and the band at 1695.4 cm^{-1} gains intensity. These two peaks are diagnostic of protein aggregation and, in particular, of the formation of antiparallel, intermolecular β-sheets (*22*, *30*, *31*). Because the absorption of aggregates is observed at 1622.6 cm^{-1}, the peak at 1625 cm^{-1} in the spectrum of native WrbA must be assigned to other structures. We propose, therefore, to assign the 1625 cm^{-1} band to WrbA oligomers.

The normalized profile of the thermal transition, as monitored at selected wavenumbers indicative of specific structural features, is reported in Figure 1c. The midpoint of thermal denaturation (T_m) lies around 55 °C. This T_m is co-incident with the midpoint for the accumulation of aggregates. Both curves are steep, and they are symmetric to each other, indicating that aggregation parallels the loss of native secondary structure. Thus, native apoWrbA is apparently converted directly to unfolded aggregates upon thermal denaturation under these conditions. The co-incident loss of α and β structures additionally implies that the native protein unfolds in a two-state manner, that is, without the detectable accumulation of intermediates, although the formation of aggregates indicates that unfolding is not an equilibrium process.

A strikingly different transition is observed for the holoprotein (Figure 1b and d). In this case, the α and β

structures are stable up to 75 °C, indicating that the cofactor remains bound during the temperature increase and that the species whose unfolding is observed is the holoprotein. The T_m in this case lies around 90 °C, indicating a dramatic effect of the cofactor in enhancing resistance to thermal unfolding. Post-transition spectra converge despite the high unfolding temperature, indicating completion of the transition. Holoprotein unfolding is accompanied, as for the apoprotein, by the accumulation of protein aggregates, again with coincident midpoint and mutually symmetric curves. However, holoprotein unfolding is not a two-state process because the profiles reported by the α-helix and β-sheet frequencies differ slightly and reproducibly. Nevertheless, as for the apoprotein, no free unfolded WrbA accumulates during thermal unfolding of the holoprotein. For both the apo and holoproteins, the thermal transitions monitored by the Amide II components at 1550 and 1530 cm^{-1}, assigned to the secondary structure and aggregates (*22*, *31*−*33*), respectively, display the same profiles as those obtained from the Amide I analysis (data not shown).

Thermal aggregation was found to be completely irreversible for both apo and holoproteins. In both cases, no residual native-like structure is detectable by FT-IR in the protein aggregates at the end of the heating protocol nor after recooling to room temperature (data not shown). The IR data thus reveal a process in which native WrbA apo and holoproteins unfold in highly cooperative transitions, and unfolded WrbA aggregates also with high cooperativity. The midpoint of the transition is shifted by almost 40 °C in the presence of bound FMN.

Detection and Characterization of Folding Intermediates by CD. The far-UV CD spectra of 30 μM apo and holoWrbA in 20 mM sodium phosphate at pH 7.2 at 20 °C are reported in Figure 2a and b. Holoprotein solutions contained 180 μM FMN, affording >98% occupancy of the bound state. The two spectra are very similar to each other and to published spectra of the apoprotein (*6*), with a minimum at 220 nm, a shoulder around 210 nm, and positive ellipticity below 205 nm. In agreement with the FT-IR results, the CD spectra indicate a well-folded α/β structure in both samples. Figure 2c shows the absorption spectrum of free FMN in the visible region, and Figure 2d shows the corresponding CD spectra of FMN, apoWrbA, and holoWrbA. Free FMN displays no CD bands at its optical absorption maxima (380 and 450 nm, due to the S2 ← S0 and S1 ← S0 electronic transitions of the monomer, respectively, and the shoulder at 475 nm, due to the S1 ← S0 transition of the dimer) (*34*). As expected, apoWrbA is devoid of CD bands in this wavelength range. The interaction of the cofactor with the protein induces pronounced CD signals at all three wavelengths. This result indicates that FMN is bound to the protein in an ordered, chiral environment. The fact that the shoulder at 475 nm is also present in the induced CD spectrum indicates that FMN can also bind to the protein as a dimer, as also reported for flavodoxin (*35*). The induced CD signals of the cofactor provide another means to monitor the interaction between WrbA and FMN.

The temperature dependence of the far-UV CD spectra of apo and holoWrbA are also shown in Figure 2a and b. The CD spectra change only slightly over the temperature range in which FT-IR spectra indicate complete unfolding and aggregation. However, the heating rate had a strong influence

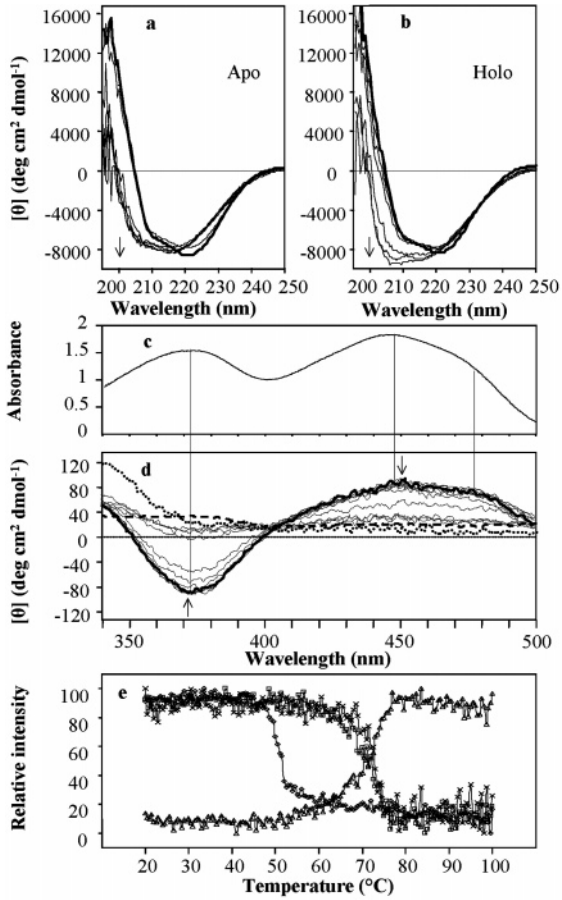

FIGURE 2: Thermal unfolding monitored by CD. (a, b) Far-UV spectra of 30 μM apo and holoWrbA at selected temperatures between 20 and 100 °C. (c) Near-UV/vis absorption spectrum of 180 μM FMN at room temperature. (d) Near-UV/vis spectra of 30 μM holoWrbA at selected temperatures between 20 and 100 °C. The arrows indicate the direction of changes with increasing temperature. In a, b, and d, the bold lines indicate spectra at 20 °C. In d, the dotted line indicates the spectrum of free FMN and the dashed line that of apoWrbA. The values are reported as mean residue ellipticity. (e) Thermal profiles at selected wavelengths. (◇), apoWrbA, 206 nm; (□), holoWrbA, 206 nm; (△), holoWrbA, 375 nm; (×), holoWrbA, 450 nm. Intensity is normalized relative to the magnitude of total signal change at each wavelength. The reported values are from one representative experiment. Variability, measured as the distance from the mean of three or four experiments, is within 6% of the values shown (two experiments at 450 nm, where data above 75 °C have variability up to 30%).

on the shape and apparent midpoint of the CD transition, as expected from the nonequilibrium thermal transitions seen by FT-IR. At low heating rates, protein aggregation and precipitation take place during the experiment, as indicated by the loss of the signal and the formation of insoluble material inside the cuvette. The solid precipitate has an FT-IR spectrum similar to the post-transition spectra of Figure 1 (data not shown). The precipitate redissolved in 6 M GuHCl has a UV−vis absorption spectrum identical to that of the apoprotein under the same conditions (data not shown), indicating that the thermal aggregates do not retain FMN. The heating rate of 0.45 °C/min employed in the experiments of Figure 2a and b represents a compromise between the speed and quality of full-wavelength spectra.

The spectral changes observed upon heating are characterized by the loss of negative ellipticity above 220 nm and the loss of positive ellipticity below 200 nm. The transition

takes place between about 45 and 50 °C for the apoprotein and between about 55 and 60 °C for the holoprotein. As in the FT-IR thermal melt, the different midpoints of thermal unfolding monitored by CD for the apo and holoproteins imply that FMN remains bound until the conformational transition occurs. The smaller shift in midpoint temperature and the smaller extent of unfolding determined by CD than by FT-IR are presumably due to the much lower protein concentrations used in the CD experiments. In addition, the temperature dependence of FMN affinity is presently unknown. Thus, in the two conditions for thermal melting, the protein could be distributed differently between apo and holo states at intermediate points of the melting curve. Also, the temperature dependence of the K_d for tetramer assembly is also unknown and can result in different dissociation states in the two samples at high temperatures. Nevertheless, the observed concentration effects imply differences in thermal stability among multimeric forms of the protein, as further documented below.

The post-transition CD spectra of apo and holoproteins exhibit a broad minimum between 200 and 220 nm and residual positive ellipticity below 200 nm (Figure 2a and b). The decrease in intensity above 220 nm is consistent with either the loss of α-helical structure or an altered contribution from tryptophan side chains within helices or both (*36*). The broad minimum below 220 is frequently seen for folded proteins with a predominantly β secondary structure (*37*). No further spectral changes are observed for either apo or holoprotein by raising the temperature to 100 °C (Figure 2 and data not shown). Thus, in the explored temperature range, the far-UV CD spectra never acquire the typical features of a fully unfolded protein. Rather, the post-transition spectra indicate the retention of substantial secondary structure at high temperatures. The spectra converge at high temperatures for each protein but differ slightly from each other, suggesting that some FMN may remain bound after the transition.

The partial unfolding of the holoprotein monitored under these conditions is nevertheless accompanied by a loss of the induced CD signals of FMN (Figure 2d). The disappearance of the band at 375 nm parallels the spectral changes monitored by far-UV CD, whereas the disappearance of the band at 450 nm is very slightly shifted toward higher temperatures. Furthermore, a small positive peak is observed at 450 nm even in the convergent post-transition spectra, whereas the spectra of both free FMN and apoprotein (Figure 4d) are featureless around that wavelength. This observation further suggests that some FMN may remain bound at high temperatures, consistent with the slight difference in the convergent post-transition far-UV CD spectra.

Fixed-wavelength measurements were carried out with a heating rate of 1 °C/min, monitoring the unfolding transition at 375 and at 206 nm, the wavelength of maximal change in far-UV ellipticity. The results are shown in Figure 2e. The T_m of the transition monitored at 206 nm is ∼51 °C for the apoprotein and ∼72 °C for the holoprotein. This result confirms the stabilizing effect of FMN toward thermal denaturation, although the shift in T_m is less remarkable than that measured by FT-IR at higher protein concentrations. The profile of the transition monitored at 375 nm is superimposable with the unfolding profile of the holoprotein obtained at 206 nm, confirming that unfolding is accompanied by the loss of the native configuration of the active-site. Because the data are normalized only to reflect the fractional change in intensity and not the fraction unfolded, the fact that the post-transition plateaus are flat indicates that no protein precipitation takes place during the experiment. Nevertheless, the transition remains poorly reversible. After heating to 100 °C, protein precipitation occurs during recooling to room temperature with the loss of the CD signal at all wavelengths (data not shown).

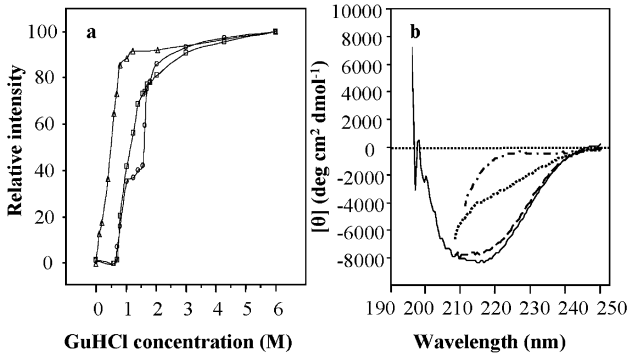

FIGURE 3: Chemical unfolding monitored by CD. (a) Denaturation profiles of apo and holoWrbA at selected wavelengths. (○), apoWrbA, 222 nm; (□), holoWrbA, 222 nm; (△), holoWrbA, 375 nm. Intensity is normalized relative to the magnitude of total signal change at each wavelength, and the values at 375 nm are multiplied by −1 for ease of comparison. The values are reported in mean residue ellipticity and are the averages from three experiments. Variability is within 8% of the mean values shown. (b) Far-UV CD spectra of apo and holoWrbA at different temperatures and GuHCl concentrations. (—), apoWrbA in 0 M GuHCl at 55 °C; (----), apoWrbA in 1.4 M GuHCl at 20 °C; (....), holoWrbA in 1.4 M GuHCl at 20 °C; (·—·), holoWrbA in 6 M GuHCl at 20 °C.

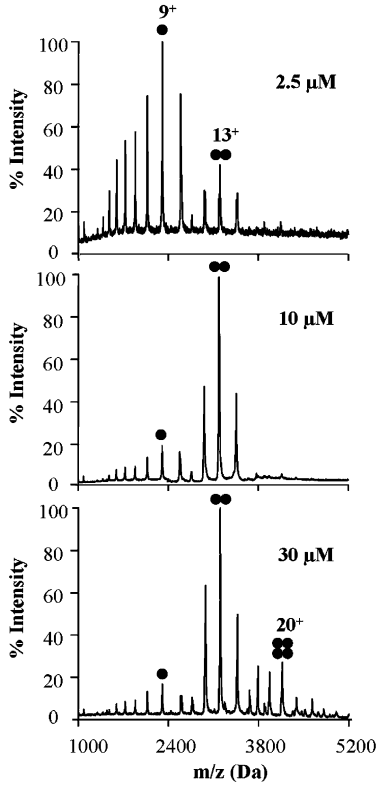

FIGURE 4: Multimerization monitored by MS. NanoESI-MS spectra at increasing concentrations of apoWrbA. The main peak of each *m/z* envelope is labeled by charge state (number of positive charges assigned to the main peak of each envelope) and by oligomeric state (each black circle represents one protein subunit).

Chemical denaturation of WrbA by guanidinium chloride (GuHCl) was monitored using the CD signals of both protein and FMN (Figure 3a). The induced CD signals of FMN at 375 nm are lost between 0 and 1 M GuHCl, before the onset of the unfolding transition monitored at 222 nm (the wavelength of maximum spectral change in the far-UV region under these conditions). Nevertheless, the profiles of protein unfolding are different for apo and holoWrbA, indicating that the species undergoing unfolding differ in the two cases. Thus, the loss of the induced CD signal at 375 nm may not correspond to the complete dissociation of FMN, as already suggested by the results of thermal unfolding. The retention of FMN by unfolded *Desulfovibrio desulfuricans* flavodoxin has also been reported, in which case residual interactions between FMN and the GuHCl-unfolded protein could be probed by calorimetry (*38*).

No overall stabilizing effect of the cofactor against chemical denaturation is observed in Figure 3a. Rather, the holoprotein is apparently less stable toward GuHCl than the apoprotein at intermediate denaturant concentrations. Although both unfolding transitions are essentially complete by 2 M GuHCl, the holoprotein unfolds in a single, relatively steep transition with a midpoint around 1 M GuHCl. Apoprotein unfolding is co-incident with the first half of the holoprotein transition but then displays a well-defined intermediate plateau followed by a second transition with a midpoint around 1.6 M GuHCl. This biphasic profile implies that partially folded forms of apoWrbA accumulate at intermediate concentrations of GuHCl, whereas chemical denaturation of the holoprotein appears to proceed without the accumulation of equilibrium folding intermediates. The distinct behaviors of apo and holoWrbA are not explained by the differences in their pre-transition oligomeric states because gel filtration generates similar elution profiles for the two proteins in 0.5 M GuHCl (apparent molecular weight 55, data not shown). The intermediate structures formed in the presence and absence of FMN must also differ. This can be inferred because if the structures were the same, then FMN binding should stabilize holoWrbA relative to apoWrba rather than destabilizing it as observed here.

The far-UV CD spectrum of the apoWrbA intermediate at 1.4 M GuHCl (Figure 3b) is almost identical to that of the thermally induced partially folded form, with a loss of intensity above 220 nm relative to the native protein and the maintenance of a broad minimum below 220 nm. Thus, both thermal and chemical denaturation generate similar partially folded forms that retain substantial secondary structure. ApoWrbA unfolding by GuHCl is only partially reversible. Spectra obtained after a 10-fold dilution from 6 M GuHCl solutions indicate 80−85% recovery of the signal at 222 nm compared to that of fresh WrbA solutions in 0.6 M GuHCl (data not shown).

Oligomerization and Ligand Binding by ESI-MS. The evidence reported above suggests that FMN may affect the oligomeric state of WrbA and that oligomerization may be a mechanism by which FMN confers enhanced thermoresistance to the protein. Previous experiments at low protein concentrations (*6*) did not detect an effect of FMN on the hydrodynamic size of WrbA. However, excess cofactor was found to increase the apparent molecular weight of 30 μM WrbA in gel filtration (data not shown). Thus, the effect of FMN on the assembly of WrbA oligomers and their relative thermal stability was further investigated by mass spectrometry. The mild ionization/desolvation conditions offered by nanoESI-MS enable the detection of intact noncovalent complexes (*39*). The high specificity of the MS signal for distinct molecular components can then be exploited to analyze supramolecular structure in complex mixtures and to detect intermediates of assembly and dissociation (*40*, *41*). Furthermore, because charge-state distribution (CSD) also reports on conformation, protein ESI-MS provides combined information about folding and binding (*42*, *43*).

Buffer conditions were first tested to optimize the detection and signal intensity of noncovalent assemblies. The experiments described below were carried out at 1 mM ammonium acetate at pH 4 because increasing the buffer concentration or the pH led to a dramatic loss of total signal intensity (data not shown). The top panel of Figure 4 shows the mass spectrum of apoWrbA at 2.5 μM total protein. The spectrum reveals one peak envelope for the monomer and one for the dimer. The CSD of the monomer is dominated by the peak of the 9+ ion with a shoulder centered around the 12+ charge state. The latter is ascribed to a partially folded form of the protein because the fully unfolded form in 10% acetic acid displays a single CSD centered around 18+ (data not shown) and because the CSDs are known to shift toward higher charge states upon unfolding (*42*). Thus, the apoprotein is not fully native under the employed experimental conditions. The mass of the protein calculated by the deconvolution of spectra obtained in 10% acetic acid is 20715.3 (±1) Da. The isotope-averaged mass calculated from the amino acid sequence is 20714.4 Da.

Mass spectra of apoWrbA display strong concentration dependence (Figure 4). As the protein concentration increases from 2.5 to 30 μM, the species distribution shifts from a prevalence of the monomer-specific envelope to a prevalence of the dimer-specific one. Already at 2.5 μM the apparent fractions of monomeric and dimeric species are approximately equal, as can be seen in Figure 4 and as confirmed by measuring peak intensities (data not shown). At the highest concentration tested (30 μM), considerable amounts of the tetramer are also detectable. These results agree with the tetrameric crystal structure of *D. radiodurans* WrbA (*21*) and with ultracentrifugation analysis showing that WrbA undergoes a monomer−dimer−tetramer equilibrium (*6*). Over the examined range of protein concentrations, the proportion of denatured protein relative to the folded monomer is approximately constant, but it progressively decreases relative to the total protein. This result suggests that oligomers are more stable than monomers.

Concentration-dependent mass spectra indicate that the observed species distribution is sensitive to the pre-existing equilibrium in solution. In contrast, when monomers are generated from complexes that dissociate during electrospray, their relative amounts are nearly independent of the original protein concentration (*43*). The data in Figure 4 indicate that the monomer−dimer transition has a midpoint between 2.5 and 10 μM, and the dimer−tetramer transition has a midpoint above 30 μM. The value for the dimer−tetramer equilibrium constant determined by analytical ultracentrifugation in 50 mM Tris HCl at pH 7.9, 0.1 M NaCl, and 10 mM $MgCl_2$ at 4 °C is approximately 1.4 μM (*6*). However, the present results cannot be directly compared with previously reported equilibrium data because the experiments

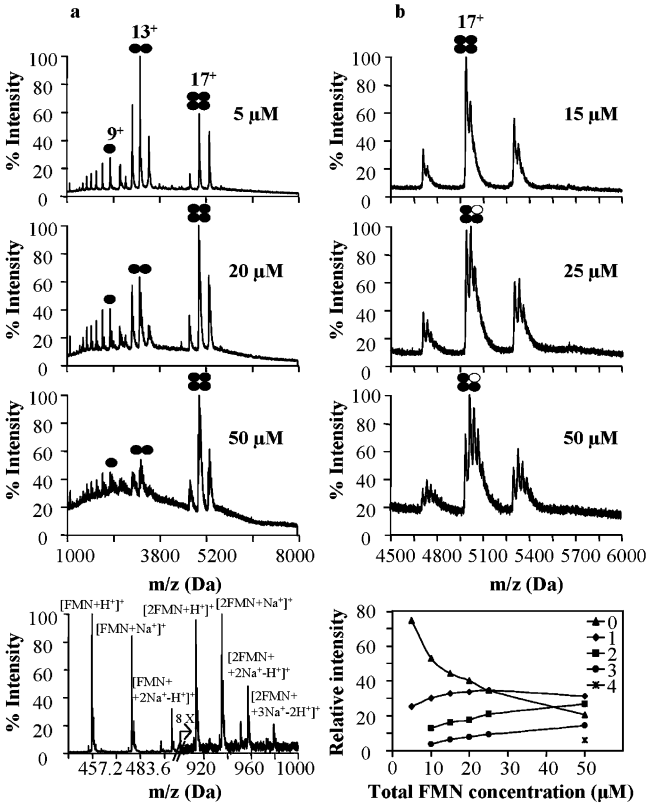

FIGURE 5: Protein−FMN interactions monitored by MS. NanoESI-MS spectra at 10 μM WrbA with increasing concentrations of FMN. Peaks are labeled as in Figure 4. All protein peaks are shown in the upper three panels of (a). The bottom panel of (a) shows the peaks of free FMN taken from the spectrum with 50 μM cofactor. In (b), the upper three panels show enlargements of the main tetramer peaks with the FMN occupancy state indicated on the main peak (○, subunit with bound FMN). The bottom panel of (b) shows the population distribution of occupancy states for WrbA tetramers with 0−4 FMN molecules bound, as measured from the intensity of adduct peaks in mass-deconvoluted spectra at 10 μM protein.

were performed at different ionic strengths, pH, and temperatures.

Ligand binding was investigated by the titration of a fixed protein concentration (10 μM) with increasing concentrations of FMN. As shown in Figure 5a, the addition of FMN induces dramatic spectral changes that indicate progressive tetramer formation at the expense of the dimer and monomer. At 25 μM FMN and above, the tetramer represents almost 100% of the molecular population, whereas, in the absence of FMN, 10 μM WrbA presents no tetrameric species (Figure 4 middle). The results indicate that FMN binding to WrbA promotes tetramer formation. Figure 5a also shows that the amount of monomer relative to the dimer remains approximately constant, whereas the amount of tetramer relative to the total protein changes from 0% to ~100%. This result indicates that FMN affects mainly the dimer−tetramer equilibrium and not the monomer−dimer equilibrium.

The comparison of the spectra reported in Figure 4 (bottom) and in Figure 5a also shows that the main charge state (most intense peak) of the tetramer is shifted from 20+ to 17+ upon the addition of FMN. This shift in CSD indicates that the holoprotein tetramer is less ionized during electrospray than the apoprotein tetramer. This shift is not observed in the comparison of apo and holodimers, and therefore, it cannot be ascribed to the negative charges of FMN. It is known that the compactness of 3D protein structures counteracts ionization during electrospray for both single molecules and noncovalent complexes (*42*). Thus, the shift in CSD suggests that the holotetramer is more compact and/or less dynamic than the apotetramer, consistent with the FT-IR results.

The fine structure of the tetramer peaks at different FMN concentrations is shown in the enlarged portion in Figure 5b. Mass heterogeneity is evident within each charge state. The average $\Delta m/z$ between adjacent peaks for the 17+ charge state is 26.7 (±0.7), implying a mass difference of 455.3 (±12) Da between adducts. This value closely matches the mass of FMN (last panel of Figure 5a; calculated monoisotopic mass of neutral FMN is 456.1 Da). Thus, all peaks differing by this mass increment presumably differ by one bound FMN. Complexes of the WrbA tetramer with 0, 1, 2, 3, and 4 molecules of FMN bound can be identified in Figure 5b, in agreement with the reported stoichiometry of 1 FMN per protein subunit (*6*, *21*). The characteristic stoichiometry of the complex revealed by the ESI-MS study emphasizes the specificity of the WrbA−FMN interaction. Very small amounts of the 1:5 complex are also detected, consistent with CD evidence that FMN can also bind to the protein as a dimer. As shown in the low m/z region of the spectrum at the bottom of Figure 5a, free FMN is also detected both as the monomer and dimer, with predominance of the monomer by a factor of ~8 at a total FMN concentration of 50 μM. This is a much larger fraction of dimeric FMN than that predicted from the previously reported dimerization equilibrium constant of approximately 10 mM in water at 25 °C (*44*). This discrepancy is presumably due to the difference in conditions.

The expected mass of the holoprotein tetramer with no FMN bound, calculated as 4 times the experimental mass of the monomer, is ~82861 Da. In Figure 5b, however, the first peak in the series of adducts, assigned to the protein with no FMN bound, has a mass of ~84796 Da. The mass of the tetramer in the apoprotein sample is also larger than expected, ~83322 Da. Discrepancies in the mass of noncovalent complexes relative to masses of their constituents can be attributed to solvent trapping at intermolecular interfaces (*39*). The solvent thus accounts for an increase in the apparent molecular weight of the tetramer of 1935 and 461 Da in the presence and absence of FMN, respectively. This result indicates that the amount of solvent trapped within the protein structure is considerably greater for the holoprotein than for the apoprotein, consistent with a less dynamic holoprotein structure.

Quantitation of the peak intensities of FMN adducts from deconvoluted mass spectra (mass as x-axis) is shown in the bottom panel of Figure 5b. The species distribution is consistent with a multistep binding process that is not strongly cooperative, in agreement with the equilibrium binding isotherm determined using fluorescence quenching in 10 mM sodium phosphate buffer at pH 7.2 (*6*). The midpoint for disappearance of the unoccupied tetramer occurs at approximately 5 μM, in the same order of magnitude as the value measured by fluorescence (~2 μM). These results suggest that the ESI process accurately samples the pre-existing solution equilibrium of FMN binding to WrbA.

Measurements at increasing nozzle temperature were performed to evaluate the relative thermostability of WrbA

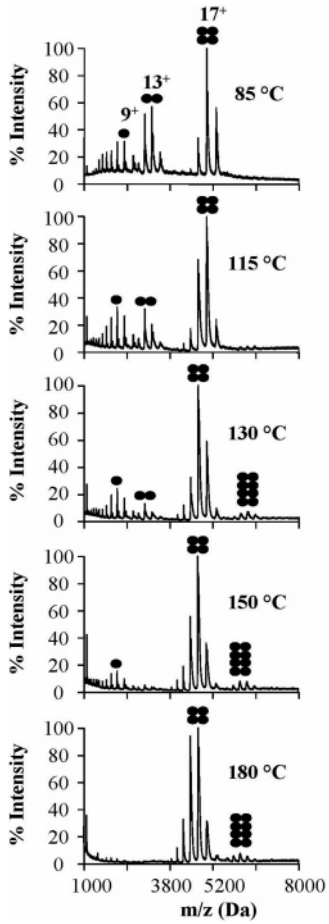

FIGURE 6: Thermal unfolding monitored by MS. NanoESI-MS spectra of 10 μM WrbA with 15 μM FMN at increasing nozzle temperature. The main peak of each envelope is labeled by charge state and oligomeric state as in Figure 4.

oligomers. Although no control on the actual droplet temperature can be achieved by this method, the observed molecular species can be compared under identical conditions. Control experiments indicate that the bulk sample in the electrospray capillary is unaffected by the nozzle temperature (data not shown), implying that the observed spectral changes are due to events taking place after droplet formation. Figure 6 shows results obtained with 10 μM protein and 15 μM FMN, a condition that allows the detection of WrbA monomers, dimers, and tetramers.

The distinct multimeric species respond uniquely to increasing the nozzle temperature from 85 to 180 °C. Monomers and dimers are selectively depleted, resulting in the detection of almost exclusively tetrameric WrbA at the highest tested temperature. This result indicates that tetramer dissociation is slow relative to the ionization/desolvation process, which occurs on the microsecond time scale. Selective depletion of monomers and dimers suggests that at higher nozzle temperatures these species unfold and aggregate and that tetramers have a higher temperature resistance than lower-order species. The intensity of tetramer-specific peaks remains almost constant in the explored temperature range. The behavior of the WrbA system during thermal treatment in ESI-MS is opposite to that observed in a similar study on bovine betalactoglobulin. In that case, dimers dissociate into folded monomers, indicating that elevated temperatures promote dissociation without inducing unfolding. For WrbA, unfolding of monomers and dimers is observed but tetramer dissociation is not. The unique responses of the two systems reinforce the conclusion that the ESI-MS measurements capture protein-specific features despite the experimental conditions.

The envelope of the tetramer CSD shifts slightly toward higher charge states at increasing temperature, indicating an increasingly dynamic and/or less compact tetramer structure. At nozzle temperatures of 130 °C and above, small peaks corresponding to WrbA octamers become detectable. This result could reflect nonspecific effects such as an enhanced signal yield of high molecular weight species due to improved desolvation at high temperature (*45*) and/or heat-promoted aggregation. Nonspecific effects can be largely ruled out, however, because these should also give rise to pentamers, hexamers, and heptamers. Thus, the presence of octamers suggests the possibility of specific interactions between WrbA tetramers. Finally, enlargement of the low-*m*/*z* regions of the spectra (not shown) indicates that the amount of apoWrbA relative to that of the holoWrbA monomer decreases slightly with increasing temperature. Assuming that the main factor affecting peak intensity is the loss of the analyte in insoluble aggregates, this result suggests a minor stabilizing effect of FMN on the WrbA monomer itself.

DISCUSSION

Complementary spectroscopic methods have been employed in this work to investigate the effect of FMN on WrbA oligomerization and stability. Because WrbA thermal unfolding is accompanied by the irreversible formation of aggregates, this study also focuses on protein aggregation. In this regard, it is instructive to compare results obtained by CD and IR. The CD signal is restricted to the contribution of molecules in solution, whereas IR also detects insoluble aggregates. However, CD is compatible with lower protein concentrations than with those required for IR. An analysis of WrbA thermal unfolding by IR spectroscopy in the temperature range 20−100 °C reveals a highly cooperative transition from the native state to insoluble aggregates without a detectable accumulation of intermediates. In contrast, a soluble, partially folded form of the protein is detectable by CD even at 100 °C. Thus, WrbA thermal unfolding seems to proceed via the formation of an aggregation-prone intermediate (Figure 7) that can be detected under the conditions of CD measurements but is too short-lived to be detected at the concentrations employed for IR spectroscopy.

As judged by CD, similar intermediates accumulate during WrbA denaturation by either heat or GuHCl, indicating a propensity of the protein to populate partially folded states during conformational transitions. The intermediate state is characterized by substantial native-like secondary structure, reminiscent of equilibrium thermal unfolding intermediates reported for some homologous flavodoxins (*46*−*48*). Thus, the formation of metastable, native-like states may be a property of the twisted, open α/β fold. In the case of WrbA, the intermediate state may be responsible for the nucleation of protein aggregates, making thermal unfolding irreversible. It is generally believed that partially folded forms are responsible for protein aggregation and that features of

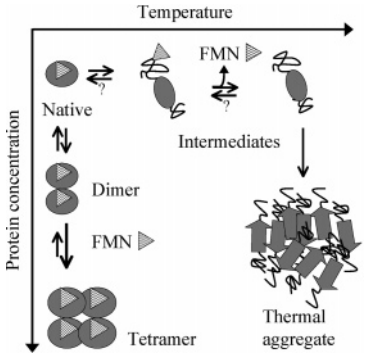

FIGURE 7: Model for the oligomerization and thermal aggregation pathways of WrbA. Monomeric native WrbA can assemble into dimers and tetramers. Tetramer formation is favored by the presence of FMN. Thermal denaturation partially unfolds the protein to an aggregation-prone intermediate that has lost the native configuration of the binding site but retains some interaction with FMN. At high protein concentrations, the intermediate undergoes further unfolding, complete dissociation from FMN, and aggregation. The intermediate is depicted as monomeric for simplicity, although no direct evidence is available on its assembly state. FMN is depicted as a triangle.

intermediates can direct protein assembly pathways toward disordered aggregates or amyloid fibrils (*49*−*51*). Thermal aggregates often form via accumulation of intermolecular antiparallel β-sheets (*22*, *30*−*32*), as observed here for apo and holoWrbA. In this case, native α-helices and intramolecular β-sheets are completely absent from the final aggregates that accumulate during IR measurements. It should be pointed out that IR spectra can reveal residual native-like secondary structures in insoluble protein aggregates when these are present, as in the inclusion bodies in recombinant bacteria (*32*, *52*, *53*).

The presence of the FMN cofactor has a dramatic effect on the T_m of WrbA, shifting it by ∼40 °C under the conditions of IR spectroscopy but with little or no effect on the structure, two results that seem contradictory. CD confirms both the thermostabilizing effect of FMN and the absence of major structural changes, although the T_m shift is less remarkable (∼20 °C), presumably due to the lower concentrations of both protein and FMN. Analysis of WrbA protein−protein and protein−ligand interactions by ESI-MS provides results that rationalize the mechanism of action of FMN in enhancing the protein's thermostability. These results clearly indicate that the cofactor acts mainly by shifting the oligomerization equilibrium toward the tetramer, which is more thermoresistant than the dimer or monomer (Figure 7). Furthermore, FMN reduces the dynamics and/or conformational heterogeneity of the tetrameric protein, as indicated by the shift of the main charge state to lower *m*/*z* in nanoESI-MS (*42*), consistent with the narrowing of the IR bands (*25*, *29*). The fact that the cofactor appears to affect tetrameric WrbA and not dimeric or monomeric WrbA provides further evidence of the specificity of the interaction. This study underscores the unique advantages of species distribution analysis by ESI-MS, which provides information that is qualitatively different from, and complementary to, that obtained by IR and CD spectroscopy.

That FMN might affect the multimerization equilibrium of WrbA had already been suggested on the basis of the crystal structure of the *D. radiodurans* complex, which displays contacts mediated by FMN across the smaller intersubunit surface. Consistent with this structural feature, the data reported here show that FMN dramatically shifts the dimer−tetramer equilibrium but leaves the monomer−dimer equilibrium almost unaffected. FMN may also exert a small influence on the thermal stability of WrbA monomers, similar to its effect on the thermal stability of the monomeric homologue *D. desulfuricans* flavodoxin (*54*). Modulation of thermoresistance by oligomerization is also implied by the numerous cases in which the proteins of thermophilic organisms display higher-order quaternary structures than their mesophilic counterparts (*55*).

In contrast to its effect on thermal denaturation, FMN has no overall stabilizing effect against chemical unfolding. The results with GuHCl suggest that the protein−ligand complex is sensitive to lower concentrations of the denaturant than to those that elicit unfolding, leading to similar unfolding midpoints for the apo and holoproteins. Nevertheless, only the apoprotein unfolds with a biphasic profile that indicates the accumulation of an equilibrium intermediate. Thus, FMN probably maintains some interactions with the protein at intermediate GuHCl concentrations rather than being completely released. Nevertheless, the ordered orientation of the ligand at the active site is lost at intermediate GuHCl concentrations, as judged from the loss of its CD signal.

The crystal structures of WrbA proteins show that each of the three moieties of FMN, the isoalloxazine ring, the ribityl tail, and the phosphate group, is contacted by residues in a contiguous chain segment (*21*). These sites may, therefore, present similar contact sites in folded and unfolded states. To produce the observed difference in stability between apo and holoWrbA, FMN must have lower affinity for the unfolded state than for the folded state. Residual cofactor binding in the denatured state is observed in proteins of several fold classes including some flavodoxins (*18*, *38*). To date only flavodoxins with relatively low FMN affinities in their folded states, similar to that of native WrbA, show FMN binding to their denatured states (*56*). Most flavodoxins have much higher FMN affinities than WrbA, and not one of them is yet reported to bind FMN in the unfolded state. Thus, high affinity is apparently neither a necessary nor a sufficient condition to promote FMN binding in the unfolded state.

REFERENCES

1. Grandori, R., and Carey, J. (1994) Six new candidate members of the α/β twisted open-sheet family detected by sequence similarity to flavodoxin, *Protein Sci. 3*, 2185−2193.
2. Yang, W., Ni, L., and Somerville, R. (1993) A stationary-phase protein of Escherichia coli that affects the mode of association between the trp repressor protein and operator-bearing DNA, *Proc. Natl. Acad. Sci. U.S.A. 90*, 5796−5800.
3. Hengge-Aronis, R. (2002) Signal transduction and regulatory mechanisms involved in control of the sigma(s) (RpoS) subunit of RNA polymerase, *Microbiol. Mol. Biol. Rev. 66*, 373−395.
4. Martinez, A., and Kolter, R. (1997) Protection of DNA during oxidative stress by the nonspecific DNA-binding protein Dps, *J. Bacteriol. 179*, 5188−5194.
5. Nöll, G., Kozma, E., Grandori, R., Carey, J., Schödl, T., Hauska, G., and Daub, J. (2005) Spectroelectrochemical investigation of the flavoprotein WrbA catalyzed by a flavin-modified gold electrode, *Langmuir 22*, 2378−2383.
6. Grandori, R., Khalifah, P., Boice, J. A., Fairman, R., Giovanielli, K., and Carey, J. (1998) Biochemical characterization of WrbA, founding member of a new family of multimeric flavodoxin-like proteins, *J. Biol. Chem. 273*, 20960−20966.

7. Patridge, E. V., and Ferry, J. G. (2006) WrbA from Escherichia coli and Archaeoglobus fulgidus is an NAD(P)H:quinone oxidoreductase, *J. Bacteriol. 188*, 3498−3506.
8. Jensen, K. A., Jr., Ryan, Z. C., Vanden, Wymelenberg, A., Cullen, D., and Hammel, K. E. (2002) An NADH:quinone oxidoreductase active during biodegradation by the brown-rot basidiomycete Gloeophyllum trabeum, *Appl. Environ. Microbiol. 68*, 2699−2703.
9. Lacour, S., and Landini, P. (2004) SigmaS-dependent gene expression at the onset of stationary phase in Escherichia coli: function of sigmaS-dependent genes and identification of their promoter sequences, *J. Bacteriol. 186*, 7186−7195.
10. Bianco, C., Imperlini, E., Calogero, R., Senatore, B., Amoresano, A., Carpentieri, A., Pucci, P., and Defez, R. (2006) Indole-3-acetic acid improves Escherichia coli's defences to stress, *Arch. Microbiol. 185*, 373−382.
11. Toone, W. M., Kuge, S., Samuels, M., Morgan, B. A., Toda, T., and Jones, N. (1998) Regulation of the fission yeast transcription factor Pap1 by oxidative stress: requirement for the nuclear export factor Crm1 (Exportin) and the stress-activated MAP kinase Sty1/Spc1, *Genes Dev. 12*, 1453−1463.
12. Shimanuki, M., Saka, Y., Yanagida, M., and Toda, T. (1995) A novel essential fission yeast gene *pad1*+ positively regulates *pap1*+-dependent transcription and is implicated in the maintenance of chromosome structure, *J. Cell Sci. 108*, 569−579.
13. Turi, T. G., Webster, P., and Rose, J. K. (1994) Brefeldin A sensitivity and resistance in Schizosaccharomyces pombe: isolation of multiple genes conferring resistance, *J. Biol. Chem. 269*, 24229−24236.
14. Toda, T., Shimanuki, M., Saka, Y., Yamano, H., Adachi, Y., Shirakawa, M., Kyogoku, Y., and Yanagida, M. (1992) Fission yeast pap1-dependent transcription is negatively regulated by an essential nuclear protein, crm1, *Mol. Cell. Biol. 12*, 5474−5484.
15. Toone, W. M., Morgan, B. A., and Jones, N. (2001) Redox control of AP-1-like factors in yeast and beyond, *Oncogene 20*, 2336−2346.
16. Grandori, R., and Carey, J. (1994) Two highly homologous putative DNA-binding proteins in yeast and E. coli, *Trends Biochem. Sci. 19*, 72.
17. Lostao, A., El Harrous, M., Daoudi, F., Romero, A., Parody-Morreale, A., and Sancho, J. (2000) Dissecting the energetics of the apoflavodoxin-FMN complex, *J. Biol. Chem. 275*, 9518−9526.
18. Higgins, C. L., Muralidhara, B. K., and Wittung-Stafshede, P. (2005) How do cofactors modulate protein folding? *Protein Pept. Lett. 12*, 165−170.
19. Ji, H.-F., Shen, L., Carey, J., Grandori, R., and Zhang, H.-Y. (2006) Weaker binding of FMN by WrbA than by flavodoxin: a molecular modeling study, *J. Mol. Struct.: THEOCHEM 764*, 155−160.
20. Sancho, J. (2006) Flavodoxins: sequence, folding, binding, function and beyond, *Cell. Mol. Life Sci. 63*, 855−864.
21. Gorman, J., and Shapiro, L. (2005) Crystal structures of the tryptophan repressor binding protein WrbA and complexes with flavin mononucleotide, *Protein Sci. 14*, 3004−3012.
22. Natalello, A., Ami, D., Brocca, S., Lotti, M., and Doglia, S. M. (2005) Secondary structure, conformational stability and glycosylation of a recombinant Candida rugosa lipase studied by Fourier-transform infrared spectroscopy, *Biochem. J. 385*, 511−517.
23. Susi, H., and Byler, D. M. (1986) Resolution-enhanced Fourier transform infrared spectroscopy of enzymes, *Methods Enzymol. 130*, 291−311.
24. Arrondo, J. L. R., and Goni, F. M. (1999) Structure and dynamics of membrane proteins as studied by infrared spectroscopy, *Prog. Biophys. Mol. Biol. 72*, 367−405.
25. Barth, A., and Zscherp, C. (2002) What vibrations tell us about proteins, *Q. Rev. Biophys. 35*, 369−430.
26. Tamm, L. K., and Tatulian, S. A. (1997) Infrared spectroscopy of proteins and peptides in lipid bilayers, *Q. Rev. Biophys. 304*, 365−429.
27. Arrondo, J. L. R., Muga, A., Castresana, J., and Goni, F. M. (1993) Quantitative studies of the structures of proteins in solution by Fourier-transform infrared spectroscopy, *Prog. Biophys. Mol. Biol. 59*, 23−56.
28. Haris, P. I., and Severcan, F. (1999) FTIR spectroscopic characterization of protein structure in aqueous and non-aqueous media, *J. Mol. Catal. B: Enzym. 7*, 207−221.
29. Manning, M. C. (2005) Use of infrared spectroscopy to monitor protein structure and stability, *Expert Rev. Proteomics 2*, 731−743.
30. Seshadri, S., Khurana, R., and Fink, A. L. (1999) Fourier transform infrared spectroscopy in analysis of protein deposits, *Methods Enzymol. 309*, 559−576.
31. Sokolowski, F., Modler, A. J., Masuch, R., Zirwer, D., Baier, M., Lutsch, G., Moss, D. A., Gast, K., and Naumann, D. (2003) Formation of critical oligomers is a key event during conformational transition of recombinant Syrian hamster prion protein, *J. Biol. Chem. 278*, 40481−40492.
32. Ami, D., Natalello, A., Taylor, G., Tonon, G., and Doglia, S. M. (2006) Structural analysis of protein inclusion bodies by Fourier transform infrared microspectroscopy, *Biochim. Biophys. Acta 1764*, 793−799.
33. Fabian, H., Choo, L.-P., Szendrei, I., Jackson, M., Halliday, W. C., Otvos, L., and Mantsch, H. H. (1993) Infrared spectroscopic characterization of Alzheimer plaques, *Appl. Spectrosc. 47*, 1513−1518.
34. Grajek, H., Zurkowska, G., Drabent, R., and Bojarski, C. (1986) The structure of the flavomononucleotide dimer, *Biochim. Biophys. Acta 881*, 241−247.
35. Muralidhara, B. K., and Wittung-Stafshede, P. (2003) Can cofactor-binding sites in proteins be flexible? *Desulfovibrio desulfuricans* flavodoxin binds FMN dimer, *Biochemistry 42*, 13074−11380.
36. Chakrabartty, A., Kortemme, T., Padmanabhan, S., and Baldwin, R. L. (1993) Aromatic side-chain contribution to far-ultraviolet circular dichroism of helical peptides and its effect on measurement of helix propensities, *Biochemistry 32*, 5560−5565.
37. Gast, K., Modler, A. J., Damaschun, H., Krober, R., Lutsch, G., Zirwer, D., Golbik, R., and Damaschun, G. (2003) Effect of environmental conditions on aggregation and fibril formation of barstar, *Eur. Biophys. J. 32*, 710−723.
38. Muralidhara, B. K., and Wittung-Stafshede, P. (2005) FMN binding and unfolding of Desulfovibrio desulfuricans flavodoxin: "hidden" intermediates at low denaturant concentrations, *Biochim. Biophys. Acta 1747*, 239−250.
39. Sobott, F., McCammon, M. G., Hernandez, H., and Robinson, C. V. (2005) The flight of macromolecular complexes in a mass spectrometer, *Philos. Trans. R. Soc. London, Ser. A 363*, 379−389.
40. Hernandez, H., and Robinson, C. V. (2001) Dynamic protein complexes: Insights from mass spectrometry, *J. Biol. Chem. 276*, 46685−46688.
41. Sobott, F., and Robinson, C. V. (2002) Protein complexes gain momentum, *Curr. Opin. Struct. Biol. 12*, 729−734.
42. Grandori, R. (2003) Electrospray-ionization mass spectrometry for protein conformational studies, *Curr. Org. Chem. 7*, 1589−1603.
43. Samalikova, M., Carey, J., and Grandori, R. (2005) Assembly of the hexameric Escherichia coli arginine repressor investigated by nano-ESI-TOF mass spectrometry, *Rapid Commun. Mass Spectrom. 19*, 2549−2552.
44. Grajek, H., Drabent, R., Zurkowska, G., and Bojarski, C. (1984) Absorption of the flavin dimers, *Biochim. Biophys. Acta 801*, 456−460.
45. Banks, F., and Whitehouse, C. M. (1996) Electrospray ionization mass spectrometry, *Methods Enzymol. 270*, 486−519.
46. van Mierlo, C. P., van Dongen, W. M., Vergeldt, F., van Berkel, W. J., and Steensma, E. (1998) The equilibrium unfolding of Azotobacter vinelandii apoflavodoxin II occurs via a relatively stable folding intermediate, *Protein Sci. 7*, 2331−2344.
47. Campos, L. A., Bueno, M., Lopez-Llano, J., Jimenez, M. A., and Sancho, J. (2004) Structure of stable protein folding intermediates by equilibrium phi-analysis: the apoflavodoxin thermal intermediate, *J. Mol. Biol. 344*, 239−255.
48. Irun, M. P., Garcia-Mira, M. M., Sanchez-Ruiz, J. M., and Sancho, J. (2001) Native hydrogen bonds in a molten globule: the apoflavodoxin thermal intermediate, *J. Mol. Biol. 306*, 877−888.
49. Dobson, C. M. (2003) Protein folding and misfolding, *Nature 426*, 884−890.
50. Khurana, R., Gillespie, J. R., Talapatra, A., Minert, L. J., Ionescu-Zanetti, C., Millett, I., and Fink, A. L. (2001) Partially folded intermediates as critical precursors of light chain amyloid fibrils and amorphous aggregates, *Biochemistry 40*, 3525−3535.
51. Uversky, V. N., and Fink, A. L. (2004) Conformational constraints for amyloid fibrillation: the importance of being unfolded, *Biochim. Biophys. Acta 1698*, 131−153.

52. Ami, D., Natalello, A., Gatti-Lafranconi, P., Lotti, M., and Doglia, S. M. (2005) Kinetics of inclusion body formation studied in intact cells by FT-IR spectroscopy, *FEBS Lett. 579*, 3433−3436.
53. Oberg, K., Chrunyk, B. A., Wetzel, R., and Fink, A. L. (1994) Native-like secondary structure in interleukin-1 beta inclusion bodies by attenuated total reflectance FTIR, *Biochemistry 33*, 2628−2634.
54. Muralidhara, B. K., and Wittung-Stafshede, P. (2004) Thermal unfolding of apo and holo *Desulfovibrio desulfuricans* flavodoxin: cofactor stabilizes folded and intermediate states, *Biochemistry 43*, 12855−12864.
55. Das, R., and Gerstein, M. (2000) The stability of thermophilic proteins: a study based on comprehensive genome comparison, *Funct. Integr. Genomics 1*, 76−88.
56. Campos, L. A., and Sancho, J. (2006) Native-specific stabilization of flavodoxin by the FMN cofactor: structural and thermodynamical explanation, *Proteins 63*, 581−594.

BI061769C